Controlling distance, size and concentration of nanoconjugates for optimized LSPR based biosensors

Ankan Dutta Chowdhury, Fahmida Nasrin, Rupali Gangopadhyay, Akhilesh Babu Ganganboina, Kenshin Takemura, Ikko Kozaki, Hiroyuki Honda, Toshimi Hara, Fuyuki Abe, Sungjo Park, Tetsuro Suzuki, Enoch Y. Park

PII: S0956-5663(20)30647-3

DOI: https://doi.org/10.1016/j.bios.2020.112657

Reference: BIOS 112657

To appear in: *Biosensors and Bioelectronics*

Received Date: 8 August 2020

Revised Date: 18 September 2020

Accepted Date: 24 September 2020

Please cite this article as: Chowdhury, A.D., Nasrin, F., Gangopadhyay, R., Ganganboina, A.B., Takemura, K., Kozaki, I., Honda, H., Hara, T., Abe, F., Park, S., Suzuki, T., Park, E.Y., Controlling distance, size and concentration of nanoconjugates for optimized LSPR based biosensors, *Biosensors and Bioelectronics* (2020), doi: https://doi.org/10.1016/j.bios.2020.112657.

CRediT authorship contribution statement

Ankan Dutta Chowdhury: Conceptualization of this study, Experimental, Investigation, Writing the manuscript. **Fahmida Nasrin and Kenshin Takemura:** Experimental. **Rupali Gangopadhyay**: Computational analysis, reviewing. **Akhilesh Babu Ganganboina:** Editing, Revising the manuscript. **Ikko Kozaki, Hiroyuki Honda, Toshimi Hara, Fuyuki Abe, Tetsuro Suzuki:** Resources. **Sungjo Park:** AFM imaging. **Enoch Y. Park:** Funding, Supervision, Revision of manuscript.

Controlling distance, size and concentration of nanoconjugates for optimized LSPR based biosensors

Ankan Dutta Chowdhury[a], Fahmida Nasrin[b], Rupali Gangopadhyay[c,#], Akhilesh Babu Ganganboina[a], Kenshin Takemura[b], Ikko Kozaki[d], Hiroyuki Honda[d], Toshimi Hara[e], Fuyuki Abe[e], Sungjo Park[f], Tetsuro Suzuki[g], Enoch Y. Park[a,b,*]

[a] *Research Institute of Green Science and Technology, Shizuoka University, 836 Ohya Suruga-ku, Shizuoka 422-8529, Japan*

[b] *Department of Bioscience, Graduate School of Science and Technology, Shizuoka University, 836 Ohya Suruga-ku, Shizuoka 422-8529, Japan*

[c] *University of Engineering and Management, Action Area III, New Town, Kolkata 100156, India*

[d] *Department of Biomolecular Engineering, Graduate School of Engineering, Nagoya University, Nagoya 464-8603, Japan*

[e] *Department of Microbiology, Shizuoka Institute of Environment and Hygiene, 4-27-2, Kita-13 Ando, Aoi-ku, Shizuoka 420-8637, Japan*

[f] *Department of Cardiovascular Medicine, Mayo Clinic College of Medicine and Science, Mayo Clinic, 200 First Street SW, Rochester, MN, 55905, U.S.A.*

[g] *Department of Infectious Diseases, Hamamatsu University School of Medicine, 1-20-115 Higashi-ku, Handa-yama, Hamamatsu 431-3192, Japan*

[*]Corresponding author. Research Institute of Green Science and Technology, Shizuoka University, 836 Ohya Suruga-ku, Shizuoka 422-8529, Japan. E-mail: park.enoch@shizuoka.ac.jp

[#]Present Address: Sister Nivedita University, DG Block (Newtown), Action Area I, 1/2, Newtown, Kolkata 700156, India

E-mail: ankan.dutta.chowdhury@shizuoka.ac.jp (A.D. Chowdhury), fahmida.nasrin.17@shizuoka.ac.jp (F. Nasrin), camrg@iacs.res.in (R. Gangopadhyay), akhilesh.babu.ganganboina@shizuoka.ac.jp (A.B. Ganganboina), takemura.kenshin16@shizuoka.ac.jp (K. Takemura), kozaki.ikkou@b.mbox.nagoya-u.ac.jp (I. Kozaki), honda@chembio.nagoya-u.ac.jp (H. Honda), toshimi1_hara@pref.shizuoka.lg.jp (T. Hara), fuyuki1_abe@pref.shizuoka.lg.jp (F. Abe), park.sungjo@mayo.edu (SP), tesuzuki@hama-med.ac.jp (T. Suzuki), park.enoch@shizuoka.ac.jp (E.Y. Park)

Abstract

In this report, we have examined the distance- and size-dependent localized surface plasmon resonance (LSPR) between fluorescent quantum dots (QDs) and adjacent gold nanoparticles (AuNPs) to provide a comprehensive evaluation, aiming for practical application in biosensing platform. A series of peptides with different chain lengths, connected between QDs and AuNPs is initially applied to prepare various CdSe QDs-peptide-AuNP systems to optimize LSPR signal. Separation distance between two nanoparticles of these systems before and after conjugation is also confirmed by quantum mechanical modeling and corroborated with their LSPR influenced fluorescence variations. After detailed optimizations, it can be noted that larger sized AuNPs make strong quenching of QDs, which gradually shows enhancement of fluorescence with the increment of distance and the smaller sized AuNPs. Depending on the requirement, it is possible to tune the optimized structure of the CdSe QD-peptide-AuNP nanostructures for the application. In this work, two different structural designs with different peptide chain length are chosen to construct two biosensor systems, observing their fluorescence enhancement and quenching effects, respectively. Using different structural orientation of these biosensors, two nanoconjugates has applied for detection of norovirus and influenza virus, respectively to confirm their application in sensing.

Keywords: Distance dependency, Localized surface plasmon resonance (LSPR), Peptide, Tunable biosensor, Virus detection

1. Introduction

Development of biosensing devices with low detection level has become extremely important (Chowdhury et al. 2019; Dutta Chowdhury et al. 2018; Hassanpour et al. 2018; Tereshchenko et al. 2017) day by day as a significant and increasing portion of the world's population is suffered every year from viral diseases. Over the last two decades, a great deal of research has been devoted to finding suitable techniques for enhancing the sensitivity of different detection platforms in biosensing (Ahmed et al. 2014; Haes and Van Duyne 2002; Nasrin et al. 2018; Qiu et al. 2017). Among these, localized surface plasmon resonance (LSPR)-based optical biosensor has emerged considerably due to its significant application potential (Acimovic et al. 2014; Adegoke et al. 2017; Brolo 2012; Jeon et al. 2018; Satija et al. 2015; Takemura et al. 2017). To improve the performance of sensing platforms, a combination of the fluorescent quantum dots (QDs) with the plasmonic metal nanoparticles has been exploited in different manners (Adegoke et al. 2017; Ganganboina and Doong 2018; Schreiber et al. 2014; Shi et al. 2015). As a detecting signal, the fluorescence intensity of QD is highly sensitive to the concentration of target analytes as well as the shape, size of the nanoparticle, refractive index, and distance between the surface polarons of adjacent metal nanoparticles (Oh et al. 2017; Pan et al. 2016) proper adjustment which is necessary for device performance. Recently, few LSPR-based fluorometric reports have claimed to achieve the desired low-level detection limit by altering the distance between the inorganic QDs and gold nanoparticles (AuNPs) (Feizpour et al. 2015). However, the successful application of the system for point-of-care detection using clinically isolated samples is not reported there. Although the parameters for optimizing LSPR are individually examined in different applications, the system has not been appropriately explored earlier. Moreover, their reliability and reproducibility also remain questionable as the parameters are not optimized in detail. Combining all the parameters in a single system, a generalized biosensing platform

can be formed for the detection of several analytes, via careful selection of their exact and optimized conditions.

In this report, a series of Cadmium Selenium (CdSe) QD-peptide-AuNP nanoconjugate systems with different peptide linkers has been designed to understand the LSPR behavior. The designed nanoconjugates were conjugated with a terminal amine, thiol, and intermediate –COOH group for binding QDs, AuNPs, and antibodies, respectively, varying the distance between nanoduos. The influence of the separation between QD and AuNP on the output of an LSPR-based sensing has been investigated using norovirus-like particles (NoV-LP) and influenza virus. Designed peptides were exposed to the detection of NoV-LPs and the influenza virus after optimizing their structure and other parameters. The efficiency of the system, using complex matrices like clinically isolated samples, has proved the system to be a potential platform for virus detection using multiple detection principles. These systems apply to the ultra-sensitive detection of small biomolecules like viruses, bacteria, proteins, etc. in a wide detection range, which is in the utmost requirement for point of care diagnosis.

2. Materials and methods

2.1. Chemicals and synthesis of peptides, antigen, and antibody

All chemical lists including antibody and virus information are given in the Supplementary material.

2.2 Preparation of water-soluble CdSe QDs

CdSe QDs were prepared according to the widely used standard protocol (Yu et al. 2003). To make the QDs in an aqueous medium, ligand exchange reaction was carried out with mercaptoacetic acid according to our previous work (Huang et al. 2007).

2.3 Seed preparation, synthesis, and growth of AuNPs:

In this report, gold nanoparticles with six different sizes (15, 25, 35, 45, 60, and 80 nm) were synthesized, and their effect on fluorescence intensity of CdSe QDs was investigated. Initially, a seed solution of AuNPs was synthesized by reducing 100 mL of 1 mM $HAuCl_4$ at pH 6.2–6.5 by dissolving 10 mL of 38.8 mM Na_3Ctr at100°C (Leng et al. 2015). A variable volume of seed solution was added with 227 μL of 44.7 mM $HAuCl_4 \cdot 3H_2O$ to synthesize the AuNPs growth solution. Finally, 176 μL of 38.8 mM $Na_3Ctr \cdot 2H_2O$ was added with continuous stirring until the color of the solution changes from colorless to wine red (Leng et al. 2015).

2.4 Preparation of the sensing probe

We have designed six peptides containing thiol group in one end and amine group in another end (listed in **Fig. S1**), which was covalently conjugated with the free carboxylic group of mercaptopropionic acid (MPA)-capped CdSe QDs by EDC/NHS chemistry eventually (Adegoke et al. 2016b). Then, AuNPs were conjugated to the end via the thiol group to prepare the QD-peptide-AuNP nanocomposite (**Scheme of Fig. 5a**). For all conjugation process between QDs and AuNPs, the concentration ratio always maintained at 2:1 as the particle size of QD is small even compared to the smallest size of AuNP used in this study. The particle numbers of these nanoparticles are calculated in 10^9 particle mL^{-1}, by the UV spectra dependent Lambert-Beers law. The mixture was stirred at 7°C for 2–3 h to synthesize the sensing probe, where the AuNPs and QDs were linked by the antibody-conjugated peptide. Before peptide linkage, EDC/NHS reaction was performed to link the

anti-NoV antibody covalently with the free carboxyl group of peptides. For the antibody binding, each of the peptides contains two carboxylic acid groups of aspartic acid (D) on its structure (**Fig. S1**). After completing the conjugation, the solution was purified by centrifuging for 5 min at 3000 × g and dissolved in 2 mL of ultrapure water.

2.5 Quantum mechanical modeling

Simulation regarding the interaction between CdSe QDs and AuNPs in CdSe QD-peptide-AuNP nanocomposites has been calculated using density functional theory (DFT) as implemented in the Gaussian 03 (Frisch et al. 2009) suite of program and given in Supplementary Material.

2.6. Physicochemical analysis and fluorometric detection of viruses using QD-peptide-AuNP sensing probe

All analytical methods, including fluorometric detection of virus-like particles are given in the Supplementary material.

3. Results and Discussion

3.1. Characterizations of AuNPs and CdSe QDs

By inoculating the various amounts of Au^{3+} solution with as-synthesized gold seeds, the AuNPs with sizes escalating from 20 to 80 nm were produced. **Fig. 1a–f** shows the typical transmission electron microscopy (TEM) images of the different AuNPs synthesized using the pH-controlled synthetic protocol. In the case of the seed solution in **Fig. 1a**, the nanoparticles are highly monodispersed in nature with an average diameter of 15.4 ± 0.5 nm. To achieve the bigger particle size with improved homogeneity, the growth reactions were

initiated simply by adding larger seed nanoparticles to the premixed solutions of Au^{3+} and sodium citrate. As shown in the TEM images of **Fig. 1b–f**, the produced AuNPs are in increasing sizes of 21, 32, 41, 65, and 80 nm, where most of the nanoparticles are in quasi-spherical shape. It is noteworthy that the calculated sizes are relatively close to their expected sizes of 25, 35, 45, 60, and 80 nm. There are very few numbers of triangular nanocrystal formed only in the case of particles above 60 nm. Ignoring the presence of these insignificant numbers of non-spherical particles, the average diameters of the AuNPs are determined and tabulated in the Table (**Fig. 1i**). We have also measured the average particle diameters of AuNP using Haiss' equation (with B1 = 3.00 and B2 = 2.20) based on the UV-vis spectra of the AuNP seeds (**Fig. 1g**) (Haiss et al. 2007). Smaller AuNPs primarily absorb the wavelength around 525 nm. With increasing the size, the absorption maxima are gradually shifted towards longer wavelengths with a significant increase in scattering. Larger spheres scatter more due to the larger optical cross-sections. Their albedo (a ratio of scattering to total extinction) increases with size, clearly indicating the successful growth of the nanoparticles. In addition, their hydrodynamic size distributions were further calculated from the dynamic light scattering (DLS) measurement (**Fig. 1h**), which also corroborated the results obtained from TEM images. The zeta potential of synthesized AuNPs also follows the expected trends of surface charges increasing along with an increase in particle sizes. The TEM image, along with size distribution, has presented in **Fig. S2.**

3.2. Effect of AuNPs size and peptide length on the fluorescence of CdSe QD-peptide-AuNP nanoconjugate

The enhancement or quenching effect of AuNPs size and peptide length on fluorescence intensities of CdSe QD-peptide-AuNP nanoconjugate is investigated. The

absorption spectra of different AuNPs display the first exciton transition peaks at 535 nm, whereas the fluorescence spectrum of CdSe QDs shows a Gaussian-shaped peak located at 638 nm (**Fig. S3**). Six different-sized AuNPs (15, 25, 35, 45, 60, and 80 nm) were linked with CdSe QDs using six different lengths of peptide linkers. Therefore, a total number of thirty-six possible combinations of CdSe QD-peptide-AuNP nanoconjugates are obtained, and their fluorescence intensities originating from CdSe QD was measured in PBS buffer at pH 6.7 (**Fig. 2a–f)**. Increasing the size of the conjugated AuNPs increased the fluorescence quenching regardless of the peptide length. In the case of 80 nm AuNP (**Fig. 2a**), the fluorescence of CdSe QDs has been completely quenched for all the nanoconjugates irrespective of the peptide length. On the other hand, with 15 nm AuNPs (**Fig. 2f**), the fluorescence of QDs is enhanced gradually as the distance between the QDs and AuNP increased from 3 nm to 18 nm, regulated by the peptide length. If QDs and AuNP are separated by a distance of 1.8 nm (6 amino acid peptide length), quenching occurred irrespective of AuNP size, while the degree of the quenching becomes stronger as the AuNP size increases (**Fig. 2a**). The smaller sized AuNPs have negligible LSPR absorption and hence quench the fluorescence emission of the QDs less effectively, following the nanometal surface energy transfer mechanism (Yun et al. 2005). Also, the local field enhancement effect of the AuNPs can enhance fluorescence emission significantly (Feng et al. 2015). However, with larger AuNPs, strong LSPR absorption bands can overlap with the emission band of the QDs. The energy transfer efficiency depends on the separation between the nanoconjugates, dominated by the dipole-dipole interaction (Zhang et al. 2014). Therefore, 80 nm AuNP displays the highest quenching efficiency due to the increased spectral overlap of the LSPR band with the emission band of CdSe QDs.

As shown in **Fig. 2a–f**, in all the nanoconjugates with QDs and AuNP separated by a distance of only 1.8 nm (shortest separated distance), exhibit quenching behavior irrespective

of AuNP sizes. However, the quenching effect is transformed into enhancement when the distance between the nanoduo (QDs and AuNP) increases from 1.8 to 15.5 nm (from 6 to 18 amino acid peptides). The quantum efficiency and the emission intensity of the CdSe QDs can be either enhanced or quenched by the equilibrium of two ways of the electron transfer process of non-radiative energy transfer (NRET) and local field enhancement effect (LFEE) (Feng et al. 2015; Zhang et al. 2014). When the nanoduo is close enough, NRET dominates, resulting in the fluorescence quenching. With the increase in the distance among the nanoduo, the LFEE becomes predominating over the NRET, contributing to the enhancement of fluorescence intensity. The emission intensity reaches the maximum at an optimal distance of about 16 nm between the particles.

3.3. Studies on bare CdSe nanostructure to build up the initial structures of peptide-CdSe QDs assembly

The goal of any simulation is to predict or analyze the real systems' properties that are not directly observable. From the quantum mechanical analysis revealed that the distance between the terminals with the bare peptide CDDK (in folded condition) was found to be around 0.4 nm, increased to 0.7 nm after linking with CdSe (~0.5–0.6 nm) in one side, and further enhanced to 0.97 nm after AuNP (0.5 nm) attachment to complete the nanoduo particle structure. Although for the sake of easy simulation, both the nanoparticles are taken in a much smaller size than their original sizes (5 nm, 35 nm), these results can qualitatively represent the behavior of the real system.

The $(CdSe)_6$ has been chosen as it is the smallest 3D cluster (D_{3d}) leading to spherical CdSe nanoparticles and retains the basic structure of $(CdSe)_N$ when $N \geq 7$. We have initially stabilized the structure of $(CdSe)_6$ with MPA. Here both O and S atoms are linked with Cd

atoms, and an eight-member ring-like structure is evolved with an S-Cd distance of 0.27 nm. This structure is unaffected when connected with a small peptide chain of X_1 (**Fig. S4a–c**), with an S-Cd distance shorter than 0.2 nm. The eight-member ring is almost retained even after AuNP is linked with the peptide-CdSe assembly when the length of the S-Cd bond is reduced by ~0.1 nm (0.26 nm). This result is in pace with the earlier finding, indicating stronger bonding of CdSe QD with the peptide chain even after the linkage of AuNP (Cui et al. 2015). With the increase in peptide chain length, the mode of CdSe QD linkage remains unchanged (via Cd atoms), and the Cd-S distance also remains almost the same (0.25 nm) while the eight-member ring is restructured to a pseudo-12-member ring (**Fig. S4**). Therefore, the attachment of CdSe with peptide is quite strong that remains unaffected by the chain length as well as the folding of the peptide chain. However, the peptide chain affects the ultimate structure of the nanoassembly and the end-to-end separation of the nanoconjugates that are reflected in the respective LSPR signal, as presented in **Fig. 3a–c**. The smallest free peptide of CDDK (X_1; **Fig. S1**) with a cumulative length of 1.8 nm, produces a folded structure in **Fig. 3a** where the end-to-end distance is calculated to be only 0.4 nm. By the successive addition of the CdSe and the smallest unit of AuNP, the distance increases up to 0.7 and 0.97 nm, respectively.

It should be noted that the simulated structures of the CdSe and the AuNP are shown here refer to the smallest possible clusters of those two. Looking at the increasing trend shown in **Fig. 3b** and **c**, it can be expected that the simulated distance between the CdSe and the AuNP becomes closer to the cumulative distance as calculated by the peptide length.

The fourth peptide of CGGGGGDGGGGDGGGGGK (X_4; **Fig S1)**, we have added the bigger cluster of AuNP (Au_8). After the attachment of the CdSe QD and AuNP, the end-to-end separation increased to 7.4 nm, which is quite close to the speculated distance of 8.5 nm, as shown in **Fig. 3d**. The fluorescence enhancement of the CdSe QD, as shown in **Fig. 3e**

also supports the prediction parallel to the simulated structures. After attachment of the AuNP on the CdSe QD-peptide assembly, the significant increase of the fluorescence indicates large enough separation of these two nanoparticles, resulting in the development of the successive LSPR. For the sensing application, we need to choose some optimized conditions. The system has some flexibility to change its electron transfer process in response to very few analytes; this is more favorable with open structure compared to the ring-like one. Keeping this in mind, the peptide X_4, harboring an open structure and 7.4 nm end-to-end separation after LSPR conjugation, offers the best possibility to switch over from enhancement to quenching behavior. This theoretical prediction will be validated through experimental results in successive sections.

3.4. Effect of AuNP concentration on the LSPR of CdSe QD-peptide-AuNP nanoconjugate

The concentration effects of CdSe QD-peptide-AuNP nanoconjugate on LSPR have been investigated in different concentrations of AuNPs, where the AuNP size is fixed at 35 nm, which is optimized in **Fig. 2d**. As shown in **Fig. 2g** in identical condition, 10^{12} AuNPs mL^{-1} had a stronger quenching effect than 10^9 AuNPs mL^{-1}, whereas the diluted solution shows better enhancement. This can be explained by the possibility of the nonspecific interaction that increases in the closeness of the AuNPs in concentrated solutions. In the case of the excess number of AuNP present in the medium, the possibility of the nonspecific surface adsorption of QDs on the surface of AuNP increases significantly, resulting in the predominant quenching effect. However, to get the optimum condition balancing the enhancement and quenching, the concentration of 10^9 AuNPs mL^{-1} should be optimal one (**Fig. 2g**), and this optimized AuNP concentration was used for further analysis.

3.5. Characterizations of CdSe QD-peptide X_4-AuNP nanoconjugate

Despite the clear indication of fluorescence enhancement or quenching after the successful conjugation of the CdSe QD-peptide-AuNP nanoconjugate, the composites were further characterized by some physicochemical tools viz. high-resolution TEM (HRTEM). In **Fig. 4a**, the small QDs (~5 nm) and the AuNPs (~35 nm) were closely oriented due to the covalent bonding and internal hydrogen bonding controlled by the peptide linkage. HRTEM image of an isolated nanocomposite deciphered the crystal fringes of the AuNP and the QDs, situated at the adjacent position (**Fig. 4b**). In the case of elemental mapping in STEM, a cluster of CdSe QD-peptideX_4-AuNP nanoconjugates has been isolated (**Fig. 4c**), in which the individual elements have been observed distinctly. The nanocomposite was mapped with Au and Cd (**Fig. 4d–e**), respectively, which revealed the successful linkage of CdSe QDs and AuNPs through the peptide linkage. Due to the small size and low molecular weight, the peptide chain was not accurately mapped. The AFM images of the nanocomposites have revealed similar observations, as mentioned in **Fig. S5**, where the AuNP and CdSe QDs are closely located in small separation, indicate the peptide linker's presence.

FTIR analysis was further carried out to reveal the involvement of the peptide in the CdSe QDs, as shown in **Fig. 4f**. In the case of the bare CdSe QDs, the spectrum appeared with all of its standard-transmitted peaks, particularly at 1541 cm^{-1} assigned to the asymmetric carboxylate (–COO–) group (Adegoke et al. 2016a). It is noteworthy that the spectrum remains almost unchanged after linking with the peptide, where some additional peaks have appeared due to the conjugation. The bands observed at 3410.1 cm^{-1}, 2903.3 cm^{-1}, and 1715.6 cm^{-1}, are recognized as –OH/NH_2 stretching, C–H stretching, and C–O stretching of carboxylic acid respectively (Tetsuka et al. 2016). The band at 1181.1 cm^{-1} represents the twisting mode of NH_3^+, which is quite common for amino acids, indicating the presence of a peptide chain (Ahmed et al. 2013).

The nanocomposites formation was further verified by hydrodynamic diameter measurement, where the CdSe QD-peptide-AuNPs nanocomposites, along with its components, were determined by DLS (**Fig. 4g**). The bare CdSe QDs and AuNPs show the hydrodynamic size of 5 ± 0.5 nm and 28.4 ± 1.5 nm, respectively, which almost matches that obtained during their initial characterizations. In the case of CdSe QD-peptide-AuNPs nanoconjugate, it shows at a diameter of 87 ± 1.5 nm, which is larger than their sizes, confirming the agglomeration. In the case of the smallest (X_1) and largest (X_4) peptides in the series, the hydrodynamic radius does not show significant changes (**Fig. S6**). But their high PDI values indicate the heterogeneous nature due to the agglomeration. The conjugation of the peptide on the CdSe QDs is also confirmed by the XPS spectra, as depicted in **Fig. 4h**. The deconvoluted C1s peak intensity has increased significantly after the addition of the peptide in the CdSe QDs. In addition, the successful conjugation of the AuNP with the CdSe QDs has also confirmed by the deconvoluted Au4f XPS spectra, as depicted in **Fig. 4i**. The Au4f peak has appeared in the spectrum of CdSe QD-peptide-AuNPs nanoconjugate, which was absent for bare CdSe QD-peptide.

3.6. Application of the optimized nanoconjugate in virus sensing

Among the fluorescence results from all the thirty-six optimized nanostructures, two CdSe QD-peptide-AuNP nanostructures with the peptide length of 7.4 nm (X_4) and 0.3 nm (X_1, **Fig. S1**) have been chosen for virus detection, employing their fluorescence enhancement and quenching effect. Before proceeding to virus detection, the control experiments of the virus particles with bare CdSe QDs, AuNPs, and CdSe QDs-peptide-AuNP without antibody conjugation were carried out to confirm any nonspecific binding (**Fig. S7**). 100 ng mL^{-1} virus solution is physically mixed with 10^9 particles mL^{-1} of bare

AuNP and CdSe QDs. The surface of AuNP adsorbed some virus particles; however, it is not significantly high to interrupt the sensing experiments. As the virus surfaces are negatively charged, it is unlikely to adsorbed on the negatively charged AuNP or CdSe QD and specifically interact with the free antibodies attached on the peptides (**Fig S7a**). The same phenomenon has also observed in the fluorescence spectra of CdSe-peptide-AuNP without antibody conjugation, eliminating the non-specific interaction of the virus (**Fig S7b**). Then the CdSe QD-peptideX_4-AuNP nanocomposite has been used to detect NoV-LPs (30–40 nm), creating steric hindrance on the path of LSPR between CdSe QDs and AuNPs (the TEM image of NoV-LP is provided in **Fig. S8**). Alternatively, quenched fluorescent CdSe QD-peptideX_1-AuNP nanocomposite has been applied to detect a relatively larger sized influenza virus (100 – 150 nm), recovering the fluorescence by obstructing the electron transfer.

3.6.1. Fluorescence quenching of CdSe QD-peptideX_4-AuNP nanoconjugates

The CdSe QD-peptideX_4-AuNP nanoconjugate shows the apparent enhancement of fluorescence compared to the bare CdSe QDs due to the LSPR-induced effect (**Fig. 5a)**. According to our hypothesis, in the present of the virus in the system, the antibodies can specifically bind to the virus. As the antibodies are situated in the transposition to each other, it can be anticipated that the bound viruses can produce enough steric repulsion to hamper the LSPR between the AuNPs and CdSe QDs (Nasrin et al. 2018). As a result, the fluorescence intensities have been gradually decreased with the increasing concentration of the NoV-LPs (**Fig. 5b**). The ratio of change in fluorescence intensities (gradually quenching) to initial fluorescence ($\Delta F/F_i$) is plotted against the virus concentration in **Fig. 5c**. Excellent linearity was observed with the increase of the NoV-LP concentration from 0.1 pg to 50 ng mL^{-1} beyond which it reaches saturation. The linearity in the concentration range of 1 pg to 100 pg

346 mL^{-1} has emphasized the calibration curve' inset. The limit of detection (LOD) is found to be
347 124 fg mL^{-1}, based on 3σ/S (σ is the standard deviation of the lowest signal, and S is the
348 slope of the linear line) (Nasrin et al. 2018). Based on these results, we expect that the
349 proposed system and the method can be an excellent alternative to the general biomolecular
350 detection by changing the entrapped antibody and its corresponding analytes.

351 To verify any nonspecific interaction or interferences from any component of the
352 sensor, the detection of the target virus was compared with other viruses and possible
353 interfering agents. The sensitivity of the CdSe QD-peptideX_4-AuNP nanocomposite is solely
354 dependent on the antibody sites and for most of the common interferants matrix effects are
355 almost negligible (**Fig. S9**). In the case of other viruses like Zika, influenza, and hepatitis E
356 virus-like particle (HEV-LP) in the same concentration of 10 pg mL^{-1}, the sensor shows an
357 almost negligible response, indicating the designed LSPR-based biosensor was highly
358 specific for the targeted NoV-LP.

359 The ultimate goal of biosensors is to detect any viral infection based on its RNA
360 measurement ability. To evaluate the applicability in clinical samples, the developed sensor
361 was further exposed to the detection of inactivated clinical NoV. RNA copy number in the
362 concentration range from 10^2 to 10^5 RNA copies mL^{-1} has been measured by the CdSe QDs-
363 peptideX_4-AuNP sensor and plotted in terms of fluorescence (**Fig. S10a**). Satisfactory
364 linearity of R^2 = 0.985 was maintained in the calibration curve (**Fig. S10b**). The LOD has
365 been calculated as 113 RNA copies mL^{-1} from the same equation, as mentioned above. The
366 linearity and low LOD prove the sensor system's ability to detect the real virus.

367

368 *3.6.2. Recovering of fluorescence intensity of CdSe QD-peptideX_1-AuNP nanoconjugates*

In the CdSe QD-peptideX_1-AuNP, a completely reverse methodology has been examined to detect the influenza virus. In contrast to the previous system, the addition of the virus to bind the antibodies should restrict the process of the LSPR between the AuNPs and CdSe QDs. To this end, the quenching effect from the AuNP is expected to be gradually lowered with the increasing concentration of the influenza virus. The results of the LSPR-induced immunofluorescence enhancement for the detection of the influenza virus (**Fig. 5d**). The corresponding linear calibration curve (**Fig. 5e**) where the LOD is found of 14.6 fg mL^{-1}, based on 3σ/S.

3.7 Spiked NoV-LP detection in serum by CdSe QD-peptideX_4-AuNP nanoconjugates

To understand the sensing capability in real sample analysis, the CdSe QD-peptideX_4-AuNP nanoconjugates have applied to a series of six samples with increasing concentrations of spiked NoV-LP in 10% serum solution followed by the calculation of the recovery using the method. As shown in **Table 1**, the recovery of 106 ± 2.5% was observed when a low concentration of 10^{-12} g mL^{-1} was spiked. 96 – 106% recovery was found when the concentration range of 10^{-12} – 5 × 10^{-10} g mL^{-1} of NoV-LPs was spiked into the serum solution. Although the matrix affects the sensor a little, which is obvious in the case of peptide and AuNP containing system, however, the relative standard deviations for all the spiking analyses are in the range of 1.4 – 3.7 % (n = 3), clearly indicating the sensing system's ability for analytical performance.

Conclusion

In this work, based on the physical significance of LSPR, we established a tunable and versatile sensing system using CdSe QD-peptide-AuNP nanoconjugate for ultrasensitive biosensing. For the detailed investigation, several CdSe QD-peptide-AuNP nanoconjugates were designed by varying the length of the peptide chain used as linker, size, and concentration of AuNPs, and the resulting changes in fluorescence intensities were examined. Theoretical simulation is performed to validate the experimental separation distance between the terminal nanoduos. The close interaction of CdSe QDs and AuNP shows a strong quenching effect of QDs fluorescence, which gradually shows enhancement of fluorescence with the increment of distance. Depending on the outcome of spectroscopic studies, two systems were chosen for the application and successfully applied for the sensing of NoV and influenza virus, respectively, using two different sized peptides, following exactly opposite sensing mechanism. In both cases, excellent linearity was observed with virus concentration with LODs of 124 fg mL^{-1} for NoV-LP and 14.6 fg mL^{-1} for the Influenza virus. In this emerging field of LSPR-based biosensing, we hope that the thorough investigation of this present study can give a useful direction in the future.

Acknowledgments

Authors thanks to Professor K. Morita of Institute of Tropical Medicine Nagasaki University and Dr. Tian-Cheng Li of National Institute of Infectious Diseases for providing the Zika virus and hepatitis E virus-like particle (HEV-LP), respectively. A.D.C. and A.B.G. sincerely thank the Japan Society for the Promotion of Science (JSPS) for a postdoctoral fellowship (Grant Nos. 17F17359 and 19F19064). R.G. acknowledges BRAF, Pune (India), for providing computational facilities.

Competing interests

The authors declare no competing interests.

Appendix A. Supplementary Materials

Supplementary materials associated with this article can be found in the online version at.

References

Acimovic, S.S., Ortega, M.A., Sanz, V., Berthelot, J., Garcia-Cordero, J.L., Renger, J., Maerkl, S.J., Kreuzer, M.P., Quidant, R., 2014. Nano Lett. 14(5), 2636–2641.

Adegoke, O., Morita, M., Kato, T., Ito, M., Suzuki, T., Park, E.Y., 2017. Biosen. Bioelectrons. 94, 513–522.

Adegoke, O., Nyokong, T., Forbes, P.B., 2016a. Luminescence 31(3), 694–703.

Adegoke, O., Seo, M.-W., Kato, T., Kawahito, S., Park, E.Y., 2016b. Biosen. Bioelectrons. 86, 135–142.

Ahmed, M.H., Byrne, J.A., McLaughlin, J., Elhissi, A., Ahmed, W., 2013. Appl. Surf. Sci. 273, 507–514.

Ahmed, S.R., Hossain, M.A., Park, J.Y., Kim, S.-H., Lee, D., Suzuki, T., Lee, J., Park, E.Y., 2014. Biosen. Bioelectrons. 58, 33–39.

Brolo, A.G., 2012. Nat. Photonics 6(11), 709.

Chowdhury, A.D., Takemura, K., Li, T.-C., Suzuki, T., Park, E.Y., 2019. Nature Commun. 10(1), 3737.

Cui, Y., Lou, Z., Wang, X., Yu, S., Yang, M., 2015. Phys Chem Chem Phys 17(14), 9222–9230.

Dutta Chowdhury, A., Ganganboina, A.B., Nasrin, F., Takemura, K., Doong, R.-a., Utomo, D.I.S., Lee, J., Khoris, I.M., Park, E.Y., 2018. Anal Chem 90(21), 12464–12474.

Feizpour, A., Yu, X., Akiyama, H., Miller, C.M., Edmans, E., Gummuluru, S., Reinhard, B.M., 2015. Small 11(13), 1592–1602.

Feng, A.L., You, M.L., Tian, L., Singamaneni, S., Liu, M., Duan, Z., Lu, T.J., Xu, F., Lin, M., 2015. Sci Rep 5, 7779.

Frisch, M., Trucks, G., Schlegel, H., Scuseria, G., Robb, M., Cheeseman, J., Scalmani, G., Barone, V., Mennucci, B., Petersson, G., 2009. Wallingford, CT 32, 5648–5652.

Ganganboina, A.B., Doong, R.-a., 2018. Sens Actuators B 273, 1179–1186.

Haes, A.J., Van Duyne, R.P., 2002. J Am Chem Soc 124(35), 10596–10604.

Haiss, W., Thanh, N.T., Aveyard, J., Fernig, D.G., 2007. Anal Chem 79(11), 4215–4221.

Hassanpour, S., Baradaran, B., de la Guardia, M., Baghbanzadeh, A., Mosafer, J., Hejazi, M., Mokhtarzadeh, A., Hasanzadeh, M., 2018. Microchim. Acta 185(12), 568.

Huang, C.-P., Li, Y.-K., Chen, T.-M., 2007. Biosen. Bioelectrons. 22(8), 1835–1838.

Jeon, J., Uthaman, S., Lee, J., Hwang, H., Kim, G., Yoo, P.J., Hammock, B.D., Kim, C.S., Park, Y.-S., Park, I.-K., 2018. Sens Actuators B 266, 710–716.

Leng, W., Pati, P., Vikesland, P.J., 2015. Environmental Science: Nano 2(5), 440–453.

Nasrin, F., Chowdhury, A.D., Takemura, K., Lee, J., Adegoke, O., Deo, V.K., Abe, F., Suzuki, T., Park, E.Y., 2018. Biosen. Bioelectrons. 122, 16–24.

Oh, S.Y., Heo, N.S., Shukla, S., Cho, H.-J., Vilian, A.E., Kim, J., Lee, S.Y., Han, Y.-K., Yoo, S.M., Huh, Y.S., 2017. Sci Rep 7(1), 10130.

Pan, M., Liang, Z., Wang, Y., Chen, Y., 2016. Sci Rep 6, 29984.

Qiu, S., Zhao, F., Zenasni, O., Li, J., Shih, W.-C., 2017. Nanoscale Horiz 2(4), 217–224.

Satija, J., Tharion, J., Mukherji, S., 2015. RSC Adv. 5(86), 69970–69979.

461 Schreiber, R., Do, J., Roller, E.-M., Zhang, T., Schüller, V.J., Nickels, P.C., Feldmann, J.,
462 Liedl, T., 2014. Nat. Nanotechnol. 9(1), 74.
463 Shi, J., Chan, C., Pang, Y., Ye, W., Tian, F., Lyu, J., Zhang, Y., Yang, M., 2015. Biosen.
464 Bioelectrons. 67, 595–600.
465 Takemura, K., Adegoke, O., Takahashi, N., Kato, T., Li, T.-C., Kitamoto, N., Tanaka, T.,
466 Suzuki, T., Park, E.Y., 2017. Biosen. Bioelectrons. 89, 998–1005.
467 Tereshchenko, A., Fedorenko, V., Smyntyna, V., Konup, I., Konup, A., Eriksson, M.,
468 Yakimova, R., Ramanavicius, A., Balme, S., Bechelany, M., 2017. Biosen. Bioelectrons.
469 92, 763–769.
470 Tetsuka, H., Nagoya, A., Fukusumi, T., Matsui, T., 2016. Adv. Mat. 28(23), 4632–4638.
471 Yu, W.W., Qu, L., Guo, W., Peng, X., 2003. Chemistry of Materials 15(14), 2854–2860.
472 Yun, C., Javier, A., Jennings, T., Fisher, M., Hira, S., Peterson, S., Hopkins, B., Reich, N.,
473 Strouse, G., 2005. J Am Chem Soc 127(9), 3115–3119.
474 Zhang, L., Song, Y., Fujita, T., Zhang, Y., Chen, M., Wang, T.H., 2014. Adv. Mat. 26(8),
475 1289–1294.

476

Graphical Abstract

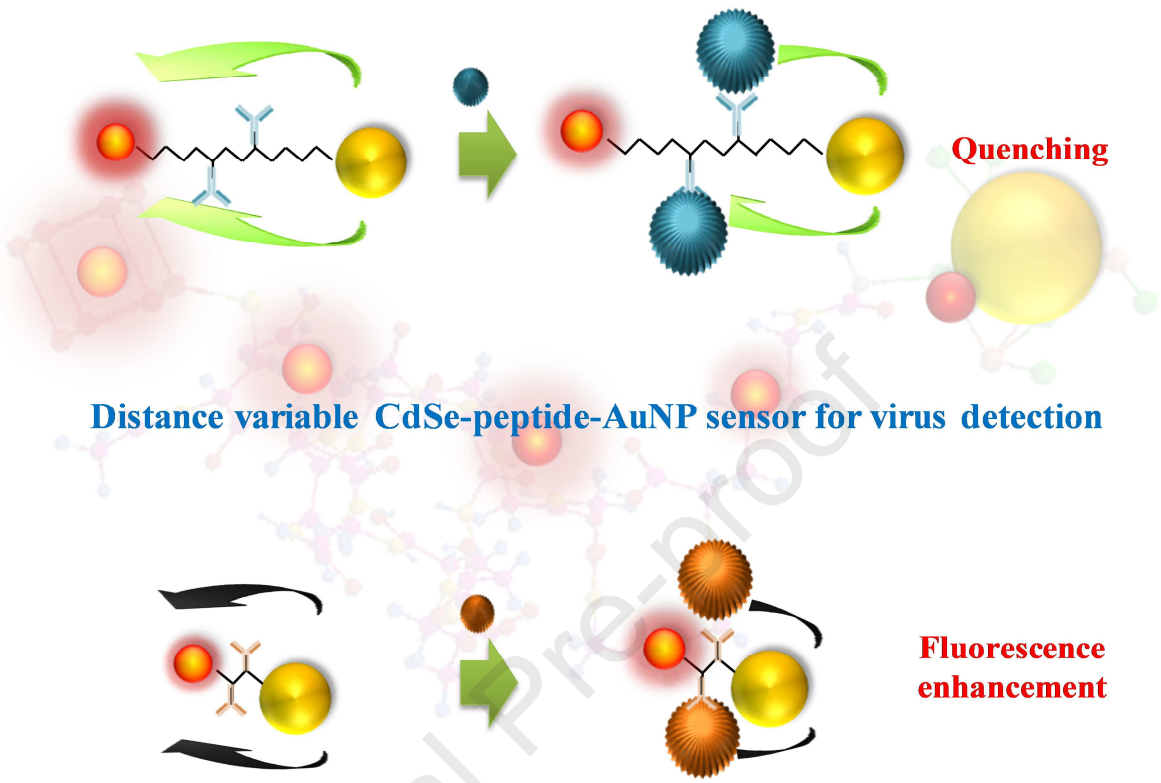

Figure captions

Fig. 1. Characterizations of different sized AuNPs. TEM images of (**a–f**) 15, 25, 35, 45, 60, and 80 nm AuNP with their corresponding daylight images and size distributions, (**g**) UV-Vis spectra and (**h**) DLS measurements of as-synthesized AuNPs, and (**i**) zeta potential values and comparative size variation of AuNPs obtained from TEM, UV-Vis, and DLS measurements.

Fig. 2. Fluorescence spectral bar diagram of CdSe QDs in various CdSe QD-peptide-AuNP nanoconjugates. Six different sizes of AuNPs at 80 nm (**a**), 60 (**b**), 45 (**c**), 35 (**d**), 25 (**e**), and 15 nm (**f**) combined with six different peptide length produced various fluorescence intensity changes. (**g**) Effect of AuNPs concentration of 10^{12}, 10^{9}, and10^{6} mL^{-1} on the nanoconjugates where all other parameters are constant.

Fig. 3. End to end distance calculation of the smallest peptide of CDDK (X_1), (**a–c**) stepwise conjugation with CdSe QD and AuNP, (**d**) simulated structure of CdSe QD-peptide X_4-AuNP, and (**e**) fluorescence spectra of the CdSe QDs and its LSPR effect after the formation of CdSe QD-peptide X_4-AuNP nanocomposite.

Fig. 4. Characterizations of CdSe QD-peptide-AuNP nanoconjugate: (**a**) TEM image (**b**) HRTEM image of CdSe QD-peptide-AuNP, showing their own fringes, (**c–e**) STEM mapping of CdSe QD-peptide-AuNP with Cd and Au, (**f**) FTIR spectra (**g**) DLS hydrodynamic distribution (**h**) XPS deconvoluted C1s spectra, and (**i**) XPS deconvoluted Au4f spectra.

Fig. 5. Virus detection with the sensor probe varying the peptide length: (**a**) schematic illustration for the virus sensing using CdSe QD-peptide-AuNP system for two modes of detection, (**b**) fluorescence emission spectra, and (**c**) corresponding calibration curve for

detection of 10^{-13} – 5×10^{-7} g mL^{-1} NoV-LP, (**d**) fluorescence emission spectra, and (**e**) corresponding calibration curves for the detection of 10^{-14} – 10^{-10} g mL^{-1} influenza viruses. The red circle in the calibration graphs indicates the blank point. Error bars denote the standard deviation of 3 replicate measurements.

509

510 **Table 1.** Recovery of NoV-LP in 10% serum samples (n = 3) by CdSe QD-peptideX_4-AuNP

511 sensing system.

Sample	Spike concentration (g mL^{-1})	Detected concentration (g mL^{-1})	Recovery ± R.S.D. (%)
Sensor	0	-	-
NoV-LPs	10^{-12}	1.06×10^{-12}	106 ± 2.5
	5×10^{-12}	5.2×10^{-12}	104 ± 1.5
	10^{-11}	9.6×10^{-12}	96 ± 1.5
	5×10^{-11}	5.1×10^{-11}	102 ± 2.3
	10^{-10}	9.7×10^{-11}	97 ± 1.4
	5×10^{-10}	5.3×10^{-10}	106 ± 3.7

512

513 **Fig. 1.**

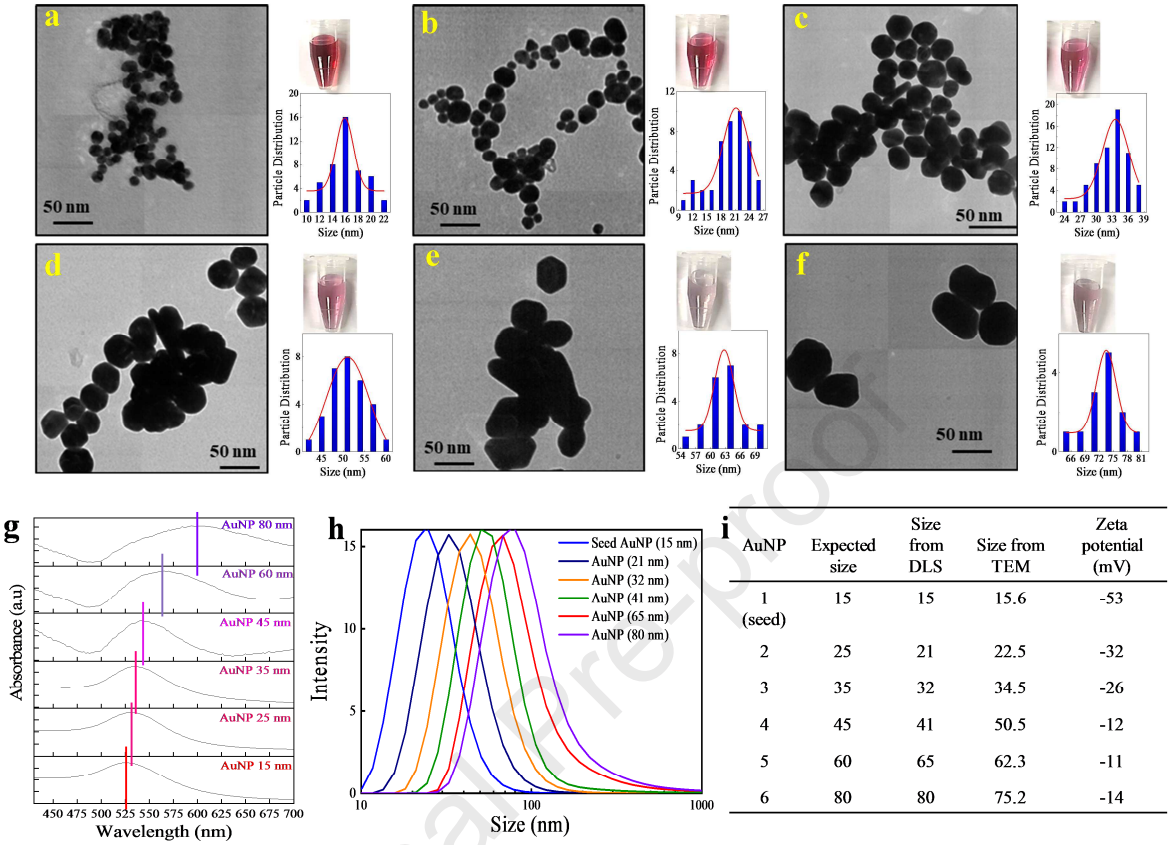

i

AuNP	Expected size	Size from DLS	Size from TEM	Zeta potential (mV)
1 (seed)	15	15	15.6	-53
2	25	21	22.5	-32
3	35	32	34.5	-26
4	45	41	50.5	-12
5	60	65	62.3	-11
6	80	80	75.2	-14

514

515

516 **Fig. 2.**

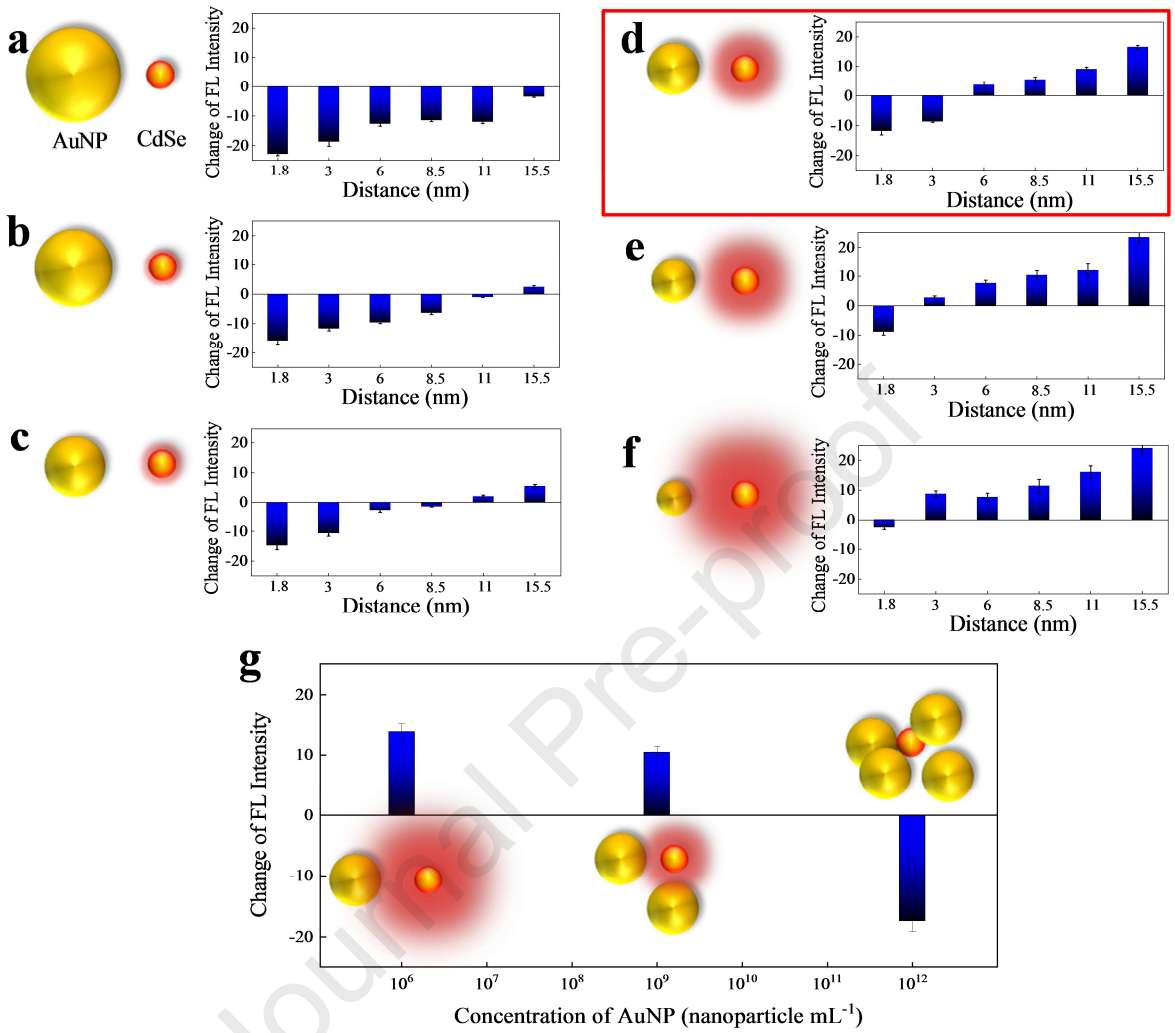

517

518

519 **Fig. 3.**

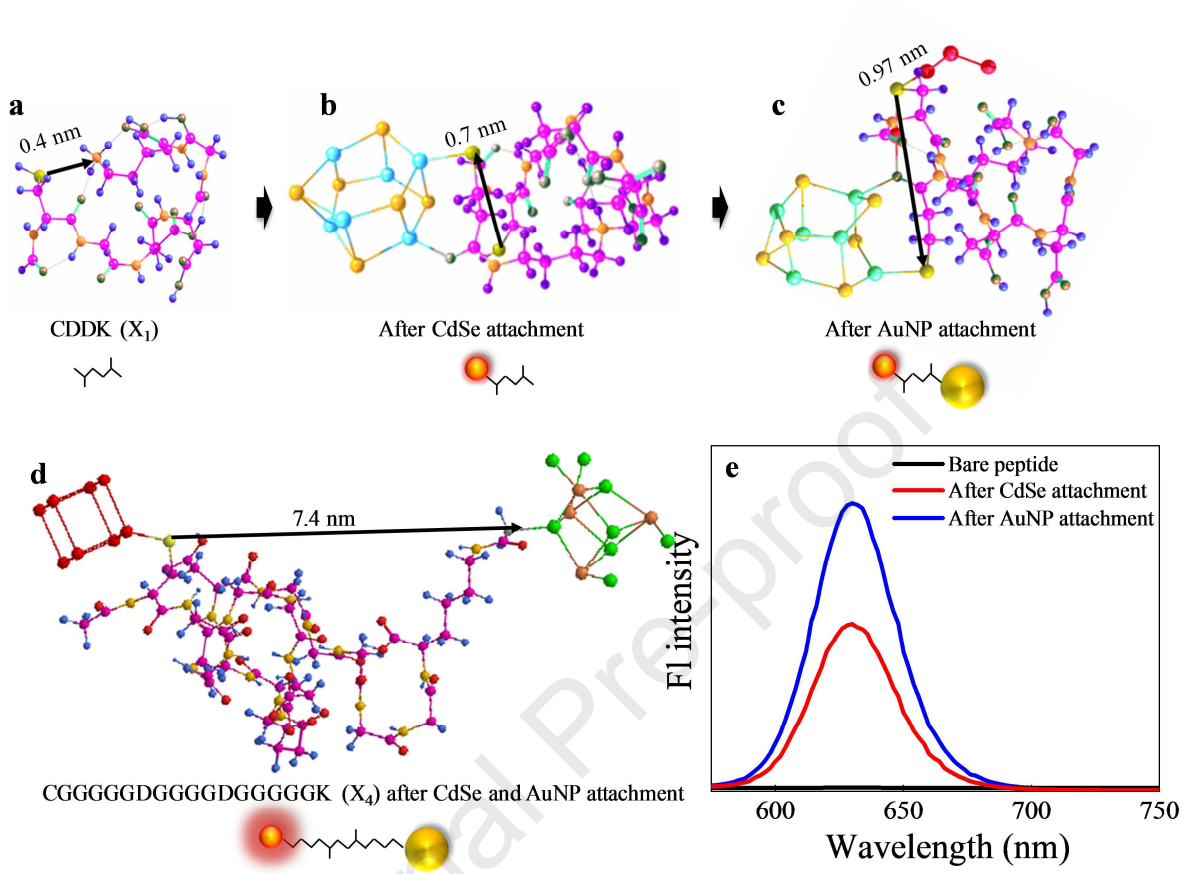

520

521

522 **Fig. 4.**

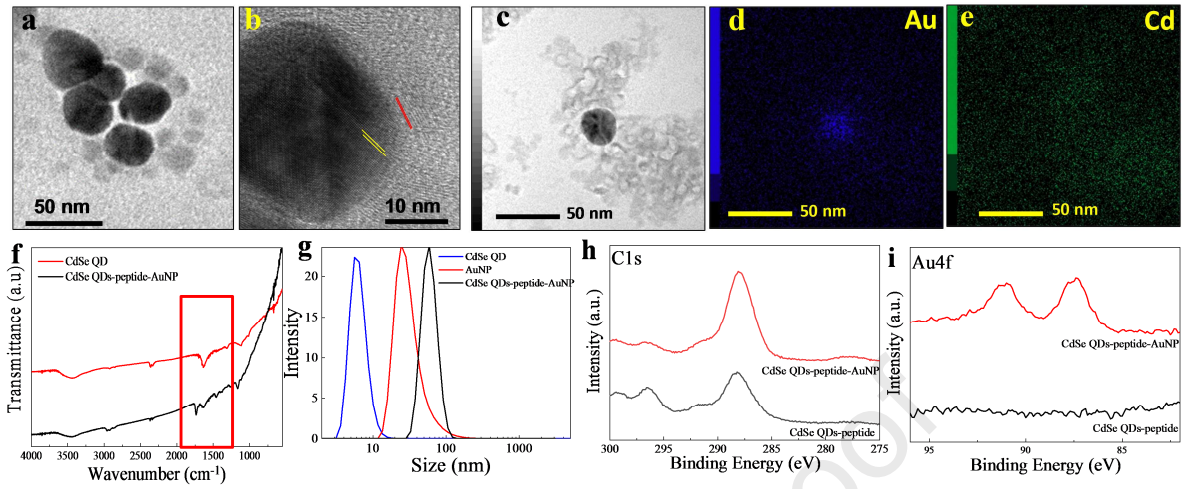

523

524

525 **Fig. 5.**

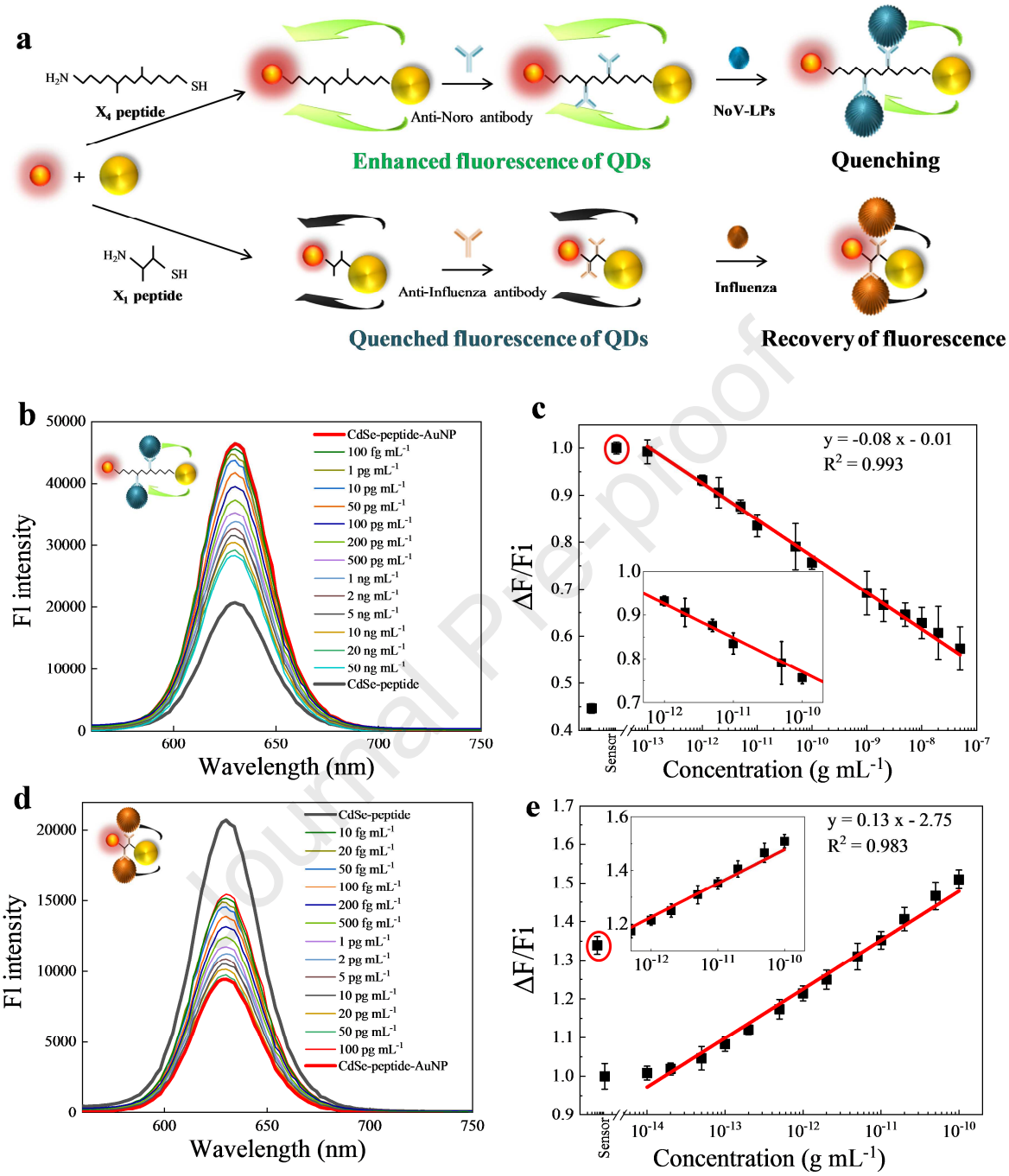

526

527

Highlights:

- A tunable system of AuNP influenced CdSe QDs fluorescence by LSPR.
- Separation between the AuNP and CdSe QDs are varied by different length peptide linkers.
- Construction of various sensor systems by detailed optimizations and simulated results.
- Application of sensors in virus detection with low LOD.

Declaration of interests

☒ The authors declare that they have no known competing financial interests or personal relationships that could have appeared to influence the work reported in this paper.

☐The authors declare the following financial interests/personal relationships which may be considered as potential competing interests: